

Gravitational-wave event rates as a new probe for dark matter microphysics

Markus R. Mosbech,^{1,*} Alexander C. Jenkins,^{2,†} Sownak Bose,^{3,‡}
Celine Boehm,^{1,§} Mairi Sakellariadou,^{4,¶} and Yvonne Y. Y. Wong^{5,**}

¹*School of Physics, The University of Sydney, Camperdown NSW 2006, Australia*

*ARC Centre of Excellence for Dark Matter Particle Physics
Sydney Consortium for Particle Physics and Cosmology*

²*Department of Physics and Astronomy, University College London, London WC1E 6BT, United Kingdom*

³*Institute for Computational Cosmology, Department of Physics,
Durham University, Durham DH1 3LE, United Kingdom*

⁴*Theoretical Particle Physics and Cosmology Group, Physics Department,
King's College London, University of London, Strand, London WC2R 2LS, United Kingdom*

⁵*School of Physics, The University of New South Wales, Sydney NSW 2052, Australia,
Sydney Consortium for Particle Physics and Cosmology*

(Dated: 12 June 2025)

We show that gravitational waves have the potential to unravel the microphysical properties of dark matter due to the dependence of the binary black hole merger rate on cosmic structure formation, which is itself highly dependent on the dark matter scenario. In particular, we demonstrate that suppression of small-scale structure—such as that caused by interacting, warm, or fuzzy dark matter—leads to a significant reduction in the rate of binary black hole mergers at redshifts $z \gtrsim 5$. This shows that future gravitational-wave observations will provide a new probe of the Λ CDM cosmological model.

I. INTRODUCTION

The standard Λ CDM model of cosmology has been posited to explain a range of observations spanning the largest observable scales to the scale of galaxies. Its success at explaining these data relies on two mysterious components: dark energy in the form of a cosmological constant (Λ) and dark matter (DM). Dark matter, in particular, is key to explaining the formation and evolution of structures such as galaxies and clusters of galaxies in the late-time Universe.

Present observations on super-galactic scales are compatible with the hypothesis that the dark matter is cold—i.e., the particles have vanishingly small thermal velocities. In this so-called cold dark matter (CDM) model, the particles also do not have significant non-gravitational interactions [1–3]; these requirements can be satisfied by a particle-like dark matter typically of mass \gtrsim keV, or a wave-like dark matter of mass $\gtrsim 10^{-22}$ eV. However, the key to determining the fundamental nature of dark matter lies in the sub-galactic scales at large redshifts. This is because the onset of non-linear structure formation can be very sensitive to the microphysics of the dark matter [4–6]. In turn, any probe that could shed light on this epoch of structure formation would also provide valuable insights into the nature of dark matter [7, 8].

There are three classes of phenomenological particle-like and wave-like dark matter scenarios that generically predict small-scale signatures that differ from the predictions of standard CDM. The first, warm dark matter (WDM) scenario usually assumes negligible interactions but has a

small DM particle mass in the low keV range that allows these particles to free-stream out of small-scale perturbations [9–19]. The second, interacting dark matter (IDM) scenario makes no strong assumption about the particle mass but endows the DM particle with non-negligible interactions (see Sec. II for details). The third, fuzzy dark matter (FDM) scenario comprises a condensate of ultra-light DM particles of mass $\sim 10^{-22}$ – 10^{-21} eV whose collective behaviour is wave-like [20]. As shown in Fig. 1, although the details differ between WDM, IDM, and FDM, all three scenarios predict a cut-off in the linear matter power spectrum at large wave numbers k , a feature that is often invoked as a possible solution to the claimed “small-scale crisis”, a long-standing set of discrepancies where simulations predict more small-scale structures than is observed [21].

In this *Letter*, we present a new observational probe of dark matter microphysics, namely the merger rate of stellar-mass binary black holes (BBHs) throughout cosmic time. With the recent advent of gravitational-wave astronomy, advanced interferometers like LIGO [22] and Virgo [23] have already detected dozens of BBHs [24, 25]. Next-generation observatories such as Einstein Telescope [26] and Cosmic Explorer [27] will be capable of detecting nearly *all* stellar-mass binary black holes in the observable Universe [28], extending the reach of gravitational-wave astronomy out to the beginning of cosmic star formation. The space-based interferometer LISA [29] will also provide a great deal of complementary low-frequency information about this population. The abundances of these systems at different epochs encode

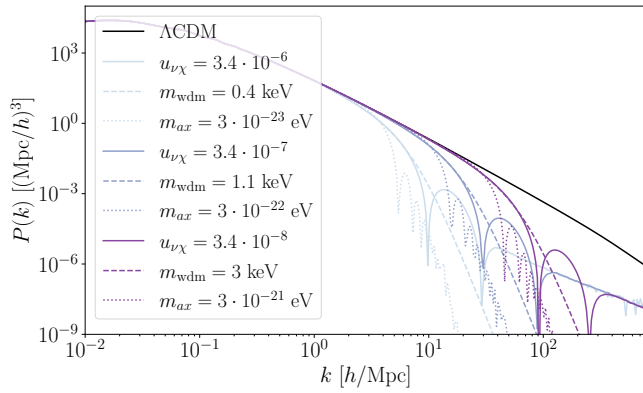


Figure 1. Linear matter power spectra for several DM-neutrino interacting scenarios of different interacting strength $u_{\nu\chi}$, along with predictions of their “equivalent” FDM and thermal WDM scenarios characterised by their respective particle masses, m_{ax} and m_{wdm} , tuned to give a similar small-scale suppression. The FDM power spectra have been computed using `AXIONCAMB` [30, 31]; the WDM power spectra are derived from the Λ CDM power spectrum filtered with a transfer function [10].

the star formation, chemical enrichment, and other baryonic processes occurring within dark matter haloes. As we demonstrate below, *the BBH merger rate is highly sensitive to the suppression of small-scale structure induced by dark matter microphysics*, as this in turn inhibits star formation and reduces the BBH yield, particularly at redshifts $z \gtrsim 5$.

In the following, we shall use as a working example a DM-neutrino interacting scenario [4, 6, 32–39] to demonstrate quantitatively the potential of the BBH merger rate to probe cosmologies with suppressed small-scale structures. A brief description of this IDM scenario is given in Sec. II. Our analysis pipeline, shown in Fig. 2, is as follows. We compute the linear matter power spectrum of an IDM cosmology using `CLASS` [38, 40, 41], which is then fed into the semi-analytic model of structure formation `GALFORM` [42, 43] to produce synthetic realisations of galactic populations, as described in Sec. III. Concurrently, we perform an N-body simulation of the IDM cosmology using the `GADGET-4` code [44, 45], initialised with the same linear input, in order to cross-check the halo mass functions predicted by `GALFORM`. Finally, the star formation rate and stellar metallicities computed by `GALFORM` are fed into the binary population synthesis code `COMPAS` [46–48], described in Sec. IV, which computes the gravitational-wave event rate. Our results and conclusions are presented in Sec. V.

Note that while we have chosen to focus on a specific IDM scenario, we expect our general conclusions to remain valid for other dark matter scenarios that predict qualitatively similar suppression of small-scale power, as non-linear evolution at $z \lesssim 10$ tends to wipe out their detailed features [49]. These include WDM and FDM as

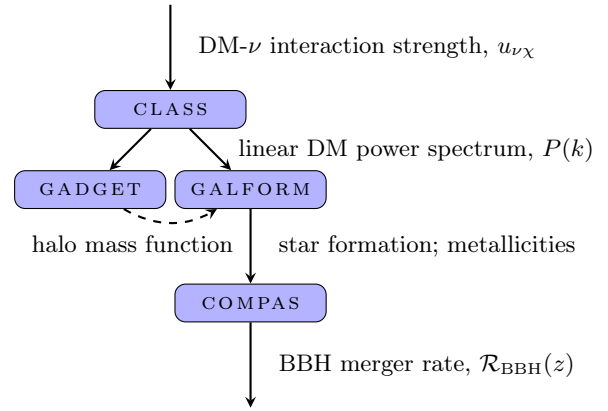


Figure 2. An illustration of our pipeline. Linear power spectra of IDM scenarios are computed using `CLASS`, which are then fed into `GADGET` and `GALFORM` as initial conditions. The `GALFORM` output is cross-checked with the halo mass function from `GADGET` and fed into `COMPAS`, which computes the gravitational-wave event rate.

already illustrated in Fig. 1, as well as DM interactions with itself [4, 6, 50–59], with photons [1, 4, 6, 37, 60–71], baryons [4, 6, 69, 70, 72–78], and dark radiation [79–90].

II. INTERACTING DARK MATTER

We consider the case in which the dark matter scatters elastically with (massive) neutrinos, via a constant, velocity-independent cross-section σ_0 as described in [38]. This kind of interaction can be realised in some particle physics theories beyond the Standard Model [5, 91–93]. From the phenomenological perspective, however, the cosmological dynamics of this interaction can be captured by a single parameter, the interaction strength, normally parameterised in terms of the dimensionless quantity [35, 36, 38, 61]

$$u_{\nu\chi} \equiv \frac{\sigma_0}{\sigma_{\text{Th}}} \left(\frac{m_\chi}{100 \text{ GeV}/c^2} \right)^{-1}, \quad (1)$$

where m_χ is the DM mass, σ_0 the interaction cross-section, and $\sigma_{\text{Th}} \approx 6.65 \times 10^{-29} \text{ m}^2$ is the Thomson scattering cross-section. The case of DM-massive neutrino interaction was previously implemented in the Einstein-Boltzmann solver `CLASS` [40, 41] in [38], which we use in this work to generate the linear matter power spectra for our IDM scenarios.

As noted earlier, the interaction suppresses the matter power spectrum below a certain scale, similar to the predictions of WDM scenarios. As collisions occur between dark matter and neutrinos, the former is prevented from collapsing to form structures, leading to a suppressed linear matter power through collisional damping. This type of damping is physically distinct from free-streaming in

WDM scenarios, where the large initial velocities result in the WDM particles escaping from initial overdensities. It is also distinct from the damping seen in FDM scenarios, which arises from quantum pressure hindering gravitational collapse. In general, the stronger the coupling, the later the DM decouples from the neutrinos and hence the larger the scales affected (see Fig. 1). Observe also that IDM scenarios predict in addition prominent acoustic oscillations at higher wave numbers. The origin of these acoustic oscillations is analogous to the baryon acoustic oscillations from the coupling of photons and baryons at early times, and the scale at which the oscillations appear is again governed by the time at which DM decouples from the neutrinos.

Cosmic microwave background (CMB) anisotropy and baryon acoustic oscillation (BAO) measurements currently constrain the DM-neutrino interaction strength to $u_{\nu\chi} \lesssim 10^{-4}$ (95% C.L.) [38]. Adding to this data set the Lyman- α forest measurements strengthens the bound to $u_{\nu\chi} \lesssim 10^{-5}$ (95% C.L.), although there also appears to be a $\sim 3\sigma$ preference for a non-zero value centred around $u_{\nu\chi} \sim 5 \times 10^{-5}$ [39]. Given these constraints on $u_{\nu\chi}$, the interaction only occurs at appreciable rates at redshifts $z \gg 1000$. At $z \lesssim 1000$, the DM particles are effectively collisionless and cold as in standard CDM, and hence amenable to standard N-body simulations of non-linear structure formation.

III. SIMULATING STRUCTURE FORMATION

Our modelling of non-linear structure is based on a combination of semi-analytic computations and N-body simulations. We use the semi-analytic model of structure formation GALFORM, first introduced in [42], which provides a flexible and computationally inexpensive way to produce synthetic realisations of galactic populations in a cosmological setting. The latest version [43] includes a large variety of astrophysical processes [94–97] to accurately model galaxy formation and evolution.

We generate merger trees using the Monte Carlo technique described in [96] (which is itself based on the extended Press-Schechter (EPS) theory, and is calibrated to the results of N-body simulations). In models in which the linear power spectrum $P(k)$ has a cut-off, as in our IDM scenario, a small correction is required to the EPS formalism: to obtain the variance of the density field $\sigma(M_{\text{halo}})$, $P(k)$ needs to be convolved with a sharp k -space filter rather than with the real-space top-hat filter used for CDM [98]. Using our Monte Carlo technique rather than N-body simulations to generate merger trees has the advantage that IDM scenarios can be studied at minimum computational expense while avoiding the complication of spurious fragmentation in filaments that occurs in N-body simulations with a resolved cut-off in $P(k)$ (e.g., [99, 100]).

We calibrate the astrophysical parameters in GAL-

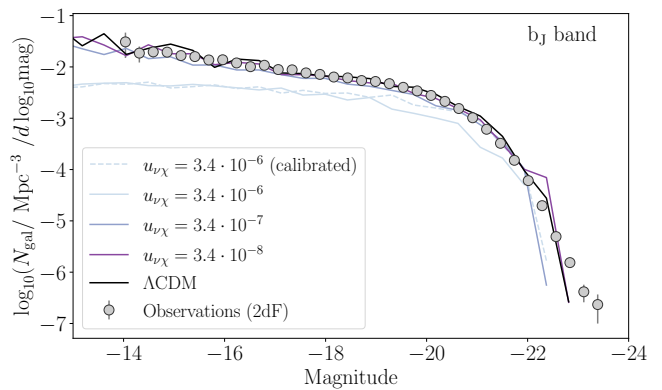


Figure 3. Galaxy luminosity functions in the b_J band for several IDM scenarios of different interaction strengths. Observational data are from the 2dF survey [101]. It is evident that while the more weakly-interacting IDM scenarios and Λ CDM are roughly consistent with observations, the $u_{\nu\chi} = 10^{-6}$ case deviates significantly. We do not show even more strongly-interacting IDM scenarios, as these deviate from observations even further.

FORM to obtain the best possible fit to observational data for Λ CDM. In particular, we adjust parameters controlling the strength of supernova feedback to achieve the best possible match to the $z = 0$ galaxy luminosity functions in the b_J and K-bands, using observational data from Refs. [101, 102]. We find that for IDM scenarios with $u_{\nu\chi} < 10^{-6}$, the same parameters used for Λ CDM provide an equally good fit to the observational data. For $u_{\nu\chi} \gtrsim 10^{-6}$, however, the feedback strength (as a function of halo mass) has to be reduced significantly to obtain the best possible fit. As shown in Fig. 3, this is still a worse fit than for the more weakly-interacting scenarios, particularly for galaxies fainter than 19th magnitude. We find that it is impossible for scenarios with $u_{\nu\chi} \gtrsim 10^{-5}$ to produce realistic galaxy distributions, since even with all astrophysical feedback mechanisms suppressing galaxy formation turned off, not enough galaxies are produced. The failure to reproduce the observed galaxy luminosity functions at $z = 0$ therefore already poses a stronger constraint on $u_{\nu\chi}$ than the previous tightest bounds from Lyman- α and rules out the preferred value found in [39].

To ensure that GALFORM accurately predicts the halo mass function of the IDM scenarios, we cross-check it by performing N-body simulations using a version of GADGET-4 [44] modified to include the effects of massive neutrinos [45] and initialised with the matter power spectra of the IDM scenarios of Fig. 1. See the Supplemental Material for details of our N-body simulations. We find that the GALFORM and N-body results are compatible with each other to the $\sim \mathcal{O}(10\%)$ level in the mass range over which we generate merger trees using the Monte Carlo technique.

IV. GRAVITATIONAL-WAVE EVENT RATES

Our key observable is the redshift-dependent BBH merger rate density $\mathcal{R}_{\text{BBH}}(z)$. In principle we could also use our simulations to study the merger rates of binary neutron stars and black hole-neutron star binaries; however, these are only detectable at lower redshifts due to their smaller masses and correspondingly weaker gravitational-wave signals. They are thus a less sensitive probe of the high-redshift suppression effects we are interested in.

Stellar-mass BBH mergers are thought to form primarily through isolated binary evolution, in which massive binary stars end their lives as black holes and radiate orbital energy through gravitational-wave emission until they eventually merge, generating an observable gravitational-wave event [103]. The BBH merger rate is thus essentially a delayed tracer of star formation, whose normalisation depends on the efficiency with which massive binary stars are converted into BBHs. This efficiency is mostly determined by the stellar metallicity (i.e., the fraction of the stellar mass that is in elements heavier than helium).

We model the merger rate using the binary population synthesis code COMPAS [46–48], which generates a synthetic BBH population by sampling individual stellar binaries from initial mass and metallicity distributions and evolving them over cosmic time. COMPAS tracks the stellar and orbital evolution of each binary, accounting for a range of physical processes such as stellar winds, mass transfer, BH formation at the end of each star’s lifetime, and subsequent shrinking of the orbit via gravitational-wave radiation reaction. We use a COMPAS dataset of 20 million evolved binaries (resulting in ≈ 0.7 million BBHs) presented in [104], which is publicly available at [105]. This gives us the BBH formation efficiency as a function of initial mass and metallicity, as well as the delay time between star formation and BBH merger. By combining this with a model for the star formation rate density and metallicity distribution as functions of redshift, we can use the COMPAS “cosmic integration” module [106] to average over the synthetic population and obtain the cosmic BBH merger rate. These inputs are typically phenomenological models chosen to fit low-redshift observational data. In our case, we instead use the star formation rates and metallicity distributions generated by GALFORM, allowing us to model how the BBH rate changes as we vary the underlying dark matter model.

One limitation of our approach is that COMPAS only accounts for BBHs formed through isolated binary evolution, neglecting other sub-dominant formation channels such as dynamical capture in dense stellar environments [103, 107] (globular clusters [108], nuclear star clusters [109], etc.) or in AGN disks [110], as well as the possible presence of primordial BBHs [111]. Note however that these additional channels can only *add* to the total merger rate, and thus have the opposite effect to dark-matter interactions;

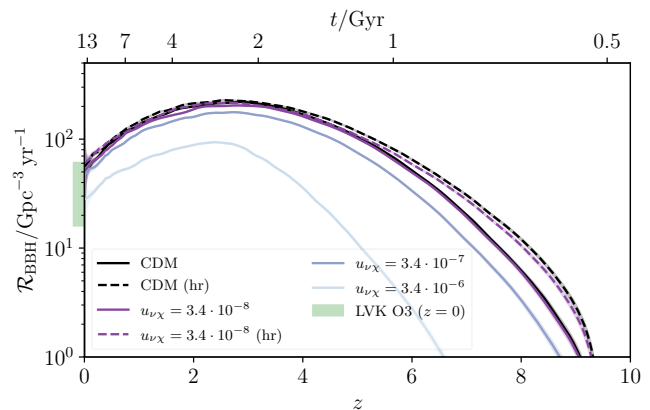


Figure 4. The binary black hole merger rate density over cosmic time, as predicted by our pipeline for Λ CDM and a range of IDM scenarios. The local $z = 0$ rate (90% C.L.) inferred from LIGO/Virgo observations [112] is shown as a green band. Lines marked ‘hr’ are high resolution, meaning that the GALFORM merger trees are tracked to smaller progenitor masses.

neglecting these additional BBHs is therefore conservative in that it cannot lead to a false-positive detection of IDM.

V. RESULTS AND DISCUSSION

Our key results for the BBH merger rate are shown in Fig. 4. In addition to the baseline Λ CDM case, we consider a range of IDM models with $u_{\nu\chi} = 3.4 \times 10^{-6}$, 3.4×10^{-7} , and 3.4×10^{-8} (recall that models with stronger DM- ν interactions than this are unable to reproduce the galaxy luminosity function data shown in Fig. 3). The factor of 3.4 comes from the CMB+BAO limits in [38]; we have chosen interaction strength values that are whole factors of 10 smaller. The rates that we obtain are dependent on the mass resolution of our GALFORM merger trees, with finer resolution allowing us to access additional star formation taking place in smaller haloes, resulting in a greater total number of BBHs. Most of the results shown in Fig. 4 use a benchmark mass resolution of $M_h \geq 10^{9.5} M_\odot$, but we additionally show results for CDM and for $u_{\nu\chi} = 3.4 \times 10^{-8}$ at a finer resolution of $M_h \geq 10^{8.5} M_\odot$. At this mass resolution, we are able to resolve the majority of the star formation in the Universe (under the assumption that it takes place through the cooling of atomic hydrogen), except for that from the ultrafaint dwarf population. We do not anticipate these galaxies to contribute significantly to the overall BBH merger rate.

All of the dark matter scenarios we consider are consistent with the local ($z = 0$) merger rate inferred by LIGO/Virgo, $\mathcal{R}_{\text{BBH}}(z = 0) = [16\text{--}61] \text{ Gpc}^{-3} \text{yr}^{-1}$ [112], with only a small suppression ($\lesssim 20\%$) of this local rate in the $u_{\nu\chi} \leq 3.4 \times 10^{-7}$ IDM scenarios compared to

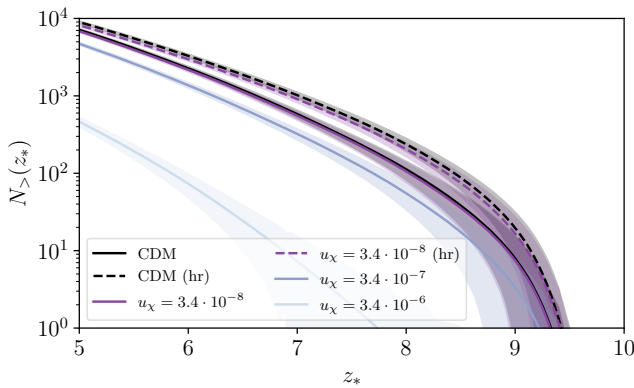


Figure 5. Expected number of BBH mergers observed with estimated redshift larger than z_* , using one year of observations with a third-generation interferometer network (Einstein Telescope plus two Cosmic Explorers), taking into account the forecasted redshift uncertainty and signal-to-noise for the expected BBH population. The shaded regions show the statistical uncertainty (99% C.L.) due to Poisson fluctuations in the number of BBHs, and ‘hr’ means high resolution, signifying that the GALFORM merger trees are tracked to smaller progenitor masses.

Λ CDM. At higher redshifts, however, we see that their differences become increasingly significant, even for the $u_{\nu\chi} = 3.4 \times 10^{-8}$ case. Physically this reflects that most star formation takes place in smaller haloes at these early epochs, and these smaller haloes are where the effects of DM interactions are most pronounced. Decreasing the interaction strength further down to $u_{\nu\chi} = 3.4 \times 10^{-9}$, however, makes the suppression scale so small that there are very few star-forming haloes that are missing compared to Λ CDM, and consequently the BBH merger rate for this scenario is essentially indistinguishable from that in Λ CDM.

In order to convince ourselves that these differences in the high- z BBH merger rate will be detectable with future gravitational-wave observatories, we compute forecasts for the expected number of BBHs, $N_>(z_*)$, detected above a given threshold redshift z_* , as well as the expected uncertainty in this quantity due to Poisson fluctuations in the number of BBHs at each redshift. (This is based on the ‘cut-and-count’ method discussed in [113]; for further details, see the Supplemental Material). We assume one year of observations with a third-generation interferometer network consisting of Einstein Telescope [114] and two Cosmic Explorers [115], accounting for the detection efficiency and redshift uncertainty associated with this network. As shown in Fig. 5, we can clearly distinguish between the different $N_>(z_*)$ predictions, allowing us to confirm or rule out a small-scale suppression of the scale caused by DM-neutrino interactions down to the level of $u_{\nu\chi} \sim 10^{-7}$.

Figure 5 clearly demonstrates that the main limitation to the cosmological information we can extract from fu-

ture gravitational-wave detections is not statistical uncertainty, but systematics associated with modelling choices. In particular, since the observational study of BBHs is still at an early stage, there are numerous astrophysical uncertainties associated with the stellar physics that governs isolated binary evolution. Here we have used the fiducial COMPAS model, but in future our analysis can be expanded by carrying out a suite of simulations in which each of the COMPAS model parameters are varied (similar to [116, 117]), allowing us to explore possible degeneracies between these and the DM-neutrino interaction strength. We stress however that there is good reason to be optimistic regarding these systematic uncertainties: any changes to the binary evolution model will have an impact at *all* redshifts and should therefore have minimal degeneracy with the specific high-redshift suppression we are targeting. We envisage that the very large numbers of BBHs detected by third-generation interferometers at low redshifts will be able to pin down the astrophysical modelling, allowing us to use the high-redshift tail as a sensitive probe of structure formation and dark matter. Similarly, we anticipate that uncertainties associated with the GALFORM modelling governing star formation and chemical enrichment will be reduced by comparing against future low-redshift observational data for faint galaxies, as well as high-redshift observations with, e.g., the James Webb Space Telescope [118].

To conclude, we have shown that the binary black hole merger rate has the potential to become an important probe of deviations from the Λ CDM model, particularly the suppression of structure from dark matter interactions. As a by-product of our analysis, we have shown that dark matter-neutrino interactions with $u_{\nu\chi} \gtrsim 10^{-6}$ are already strongly in tension with the observed abundance of faint galaxies. With the next generation of gravitational-wave observatories probing the gravitational-wave event rate out to the earliest epochs of star formation, it will be possible to strengthen these constraints by another order of magnitude or more, giving us highly sensitive information about the earliest stages of non-linear structure formation.

AUTHOR CONTRIBUTIONS

The idea for this project was proposed by CB, MS and ACJ. MM performed the N-body simulations, halo-finding, and halo mass function analysis with input from YW, SB computed the galaxy populations, and ACJ made the gravitational-wave predictions. All authors contributed to every stage of the paper, including the writing.

ACKNOWLEDGMENTS

The authors would like to thank Joe Silk for useful discussions, and Ilya Mandel for helpful correspondence about COMPAS. MS thanks the University of Sydney for its hospitality during the early stages of this project. SB is supported by the UK Research and Innovation (UKRI) Future Leaders Fellowship [grant number MR/V023381/1]. MS is supported in part by the Science and Technology Facility Council (STFC), United Kingdom, under the research grant ST/P000258/1. Y³W is supported in part by the Australian Government through the Australian Research Council’s Future Fellowship (project FT180100031). The authors acknowledge the Sydney Informatics Hub and the use of the University of Sydney’s high performance computing cluster, Artemis. This work used the DiRAC@Durham facility managed by the Institute for Computational Cosmology on behalf of the STFC DiRAC HPC Facility (www.dirac.ac.uk). The equipment was funded by BEIS capital funding via STFC capital grants ST/P002293/1, ST/R002371/1 and ST/S002502/1, Durham University and STFC operations grant ST/R000832/1. DiRAC is part of the National e-Infrastructure. This work was partly enabled by the UCL Cosmoparticle Initiative. Simulations in this paper made use of the COMPAS rapid binary population synthesis code (version 02.21.00), which is freely available at <http://github.com/TeamCOMPAS/COMPAS>. This paper has an Einstein Telescope number ET-0171A-22.

* markus.mosbech@sydney.edu.au

† alex.jenkins@ucl.ac.uk

‡ sownak.bose@durham.ac.uk

§ celine.boehm@sydney.edu.au

¶ mairi.sakellariadou@kcl.ac.uk

** yvonne.y.wong@unsw.edu.au

- [1] C. Boehm, A. Riazuelo, S. H. Hansen, and R. Schaeffer, *Phys. Rev. D* **66**, 083505 (2002), [arXiv:astro-ph/0112522](https://arxiv.org/abs/hep-ph/0112522).
- [2] N. Aghanim *et al.* (Planck), *Astron. Astrophys.* **641**, A1 (2020), [arXiv:1807.06205](https://arxiv.org/abs/1807.06205) [astro-ph.CO].
- [3] P. Bull *et al.*, *Phys. Dark Univ.* **12**, 56 (2016), [arXiv:1512.05356](https://arxiv.org/abs/1512.05356) [astro-ph.CO].
- [4] C. Boehm, P. Fayet, and R. Schaeffer, *Phys. Lett. B* **518**, 8 (2001), [arXiv:astro-ph/0012504](https://arxiv.org/abs/hep-ph/0012504) [astro-ph].
- [5] C. Boehm, H. Mathis, J. Devriendt, and J. Silk, *Mon. Not. Roy. Astron. Soc.* **360**, 282 (2005), [arXiv:astro-ph/0309652](https://arxiv.org/abs/hep-ph/0309652).
- [6] C. Boehm and R. Schaeffer, *Astron. Astrophys.* **438**, 419 (2005), [arXiv:astro-ph/0410591](https://arxiv.org/abs/hep-ph/0410591) [astro-ph].
- [7] I. P. Carucci, F. Villaescusa-Navarro, M. Viel, and A. Lapi, *JCAP* **07**, 047 (2015), [arXiv:1502.06961](https://arxiv.org/abs/1502.06961) [astro-ph.CO].
- [8] S. Chakrabarti *et al.*, in *2022 Snowmass Summer Study* (2022) [arXiv:2203.06200](https://arxiv.org/abs/2203.06200) [astro-ph.CO].
- [9] S. Dodelson and L. M. Widrow, *Phys. Rev. Lett.* **72**, 17 (1994), [arXiv:hep-ph/9303287](https://arxiv.org/abs/hep-ph/9303287).
- [10] P. Bode, J. P. Ostriker, and N. Turok, *Astrophys. J.* **556**, 93 (2001), [arXiv:astro-ph/0010389](https://arxiv.org/abs/hep-ph/0010389).
- [11] S. H. Hansen, J. Lesgourgues, S. Pastor, and J. Silk, *Mon. Not. Roy. Astron. Soc.* **333**, 544 (2002), [arXiv:astro-ph/0106108](https://arxiv.org/abs/hep-ph/0106108).
- [12] T. Asaka, S. Blanchet, and M. Shaposhnikov, *Phys. Lett. B* **631**, 151 (2005), [arXiv:hep-ph/0503065](https://arxiv.org/abs/hep-ph/0503065).
- [13] M. Viel, J. Lesgourgues, M. G. Haehnelt, S. Matarrese, and A. Riotto, *Phys. Rev. D* **71**, 063534 (2005), [arXiv:astro-ph/0501562](https://arxiv.org/abs/hep-ph/0501562).
- [14] A. Boyarsky, O. Ruchayskiy, and M. Shaposhnikov, *Ann. Rev. Nucl. Part. Sci.* **59**, 191 (2009), [arXiv:0901.0011](https://arxiv.org/abs/hep-ph/0901.0011) [hep-ph].
- [15] M. Viel, G. D. Becker, J. S. Bolton, and M. G. Haehnelt, *Phys. Rev. D* **88**, 043502 (2013), [arXiv:1306.2314](https://arxiv.org/abs/1306.2314) [astro-ph.CO].
- [16] K. Abazajian, G. M. Fuller, and M. Patel, *Phys. Rev. D* **64**, 023501 (2001), [arXiv:astro-ph/0101524](https://arxiv.org/abs/hep-ph/0101524).
- [17] A. Boyarsky, J. Lesgourgues, O. Ruchayskiy, and M. Viel, *JCAP* **05**, 012 (2009), [arXiv:0812.0010](https://arxiv.org/abs/hep-ph/0812.0010) [astro-ph].
- [18] A. Dolgov and S. Hansen, *Astropart. Phys.* **16**, 339 (2002), [arXiv:hep-ph/0009083](https://arxiv.org/abs/hep-ph/0009083).
- [19] S. Bose, W. A. Hellwing, C. S. Frenk, A. Jenkins, M. R. Lovell, J. C. Helly, and B. Li, *Mon. Not. Roy. Astron. Soc.* **455**, 318 (2016), [arXiv:1507.01998](https://arxiv.org/abs/1507.01998) [astro-ph.CO].
- [20] L. Hui, *Ann. Rev. Astron. Astrophys.* **59**, 247 (2021), [arXiv:2101.11735](https://arxiv.org/abs/2101.11735) [astro-ph.CO].
- [21] J. S. Bullock and M. Boylan-Kolchin, *Ann. Rev. Astron. Astrophys.* **55**, 343 (2017), [arXiv:1707.04256](https://arxiv.org/abs/1707.04256) [astro-ph.CO].
- [22] J. Aasi *et al.* (LIGO), *Class. Quant. Grav.* **32**, 074001 (2015), [arXiv:1411.4547](https://arxiv.org/abs/1411.4547) [gr-qc].
- [23] F. Acernese *et al.* (Virgo), *Class. Quant. Grav.* **32**, 024001 (2015), [arXiv:1408.3978](https://arxiv.org/abs/1408.3978) [gr-qc].
- [24] R. Abbott *et al.* (LIGO, Virgo), (2021), [arXiv:2108.01045](https://arxiv.org/abs/2108.01045) [gr-qc].
- [25] R. Abbott *et al.* (LIGO, Virgo, KAGRA), (2021), [arXiv:2111.03606](https://arxiv.org/abs/2111.03606) [gr-qc].
- [26] M. Punturo *et al.*, *Class. Quant. Grav.* **27**, 194002 (2010).
- [27] D. Reitze *et al.*, *Bull. Am. Astron. Soc.* **51**, 035 (2019), [arXiv:1907.04833](https://arxiv.org/abs/1907.04833) [astro-ph.IM].
- [28] T. Regimbau, M. Evans, N. Christensen, E. Katsavounidis, B. Sathyaprakash, and S. Vitale, *Phys. Rev. Lett.* **118**, 151105 (2017), [arXiv:1611.08943](https://arxiv.org/abs/1611.08943) [astro-ph.CO].
- [29] P. Amaro-Seoane *et al.* (LISA), (2017), [arXiv:1702.00786](https://arxiv.org/abs/1702.00786) [astro-ph.IM].
- [30] R. Hlozek, D. Grin, D. J. E. Marsh, and P. G. Ferreira, *Phys. Rev. D* **91**, 103512 (2015), [arXiv:1410.2896](https://arxiv.org/abs/1410.2896) [astro-ph.CO].
- [31] D. Grin, D. J. E. Marsh, and R. Hlozek, “axionCAMB: Modification of the CAMB Boltzmann code,” *Astrophysics Source Code Library*, record ascl:2203.026 (2022), [ascl:2203.026](https://arxiv.org/abs/ascl:2203.026).
- [32] G. Mangano, A. Melchiorri, P. Serra, A. Cooray, and M. Kamionkowski, *Phys. Rev. D* **74**, 043517 (2006), [arXiv:astro-ph/0606190](https://arxiv.org/abs/hep-ph/0606190) [astro-ph].
- [33] P. Serra, F. Zalamea, A. Cooray, G. Mangano, and A. Melchiorri, *Phys. Rev. D* **81**, 043507 (2010), [arXiv:0911.4411](https://arxiv.org/abs/hep-ph/0911.4411) [astro-ph.CO].

- [34] R. J. Wilkinson, C. Boehm, and J. Lesgourgues, *JCAP* **1405**, 011 (2014), arXiv:1401.7597 [astro-ph.CO].
- [35] E. Di Valentino, C. Boehm, E. Hivon, and F. R. Bouchet, *Phys. Rev. D* **97**, 043513 (2018), arXiv:1710.02559 [astro-ph.CO].
- [36] J. Stadler, C. Boehm, and O. Mena, *JCAP* **08**, 014 (2019), arXiv:1903.00540 [astro-ph.CO].
- [37] Y. Ali-Haïmoud, J. Chluba, and M. Kamionkowski, *Phys. Rev. Lett.* **115**, 071304 (2015), arXiv:1506.04745 [astro-ph.CO].
- [38] M. R. Mosbech, C. Boehm, S. Hannestad, O. Mena, J. Stadler, and Y. Y. Y. Wong, *JCAP* **03**, 066 (2021), code available at https://github.com/MarkMos/CLASS_nu-DM, arXiv:2011.04206 [astro-ph.CO].
- [39] D. C. Hooper and M. Lucca, *Phys. Rev. D* **105**, 103504 (2022), arXiv:2110.04024 [astro-ph.CO].
- [40] D. Blas, J. Lesgourgues, and T. Tram, *JCAP* **07**, 034 (2011), arXiv:1104.2933 [astro-ph.CO].
- [41] J. Lesgourgues and T. Tram, *JCAP* **09**, 032 (2011), arXiv:1104.2935 [astro-ph.CO].
- [42] S. Cole, C. G. Lacey, C. M. Baugh, and C. S. Frenk, *Mon. Not. Roy. Astron. Soc.* **319**, 168 (2000), astro-ph/0007281.
- [43] C. G. Lacey, C. M. Baugh, C. S. Frenk, A. J. Benson, R. G. Bower, S. Cole, V. Gonzalez-Perez, J. C. Helly, C. D. P. Lagos, and P. D. Mitchell, *Mon. Not. Roy. Astron. Soc.* **462**, 3854 (2016), arXiv:1509.08473 [astro-ph.GA].
- [44] V. Springel, R. Pakmor, O. Zier, and M. Reinecke, *Mon. Not. Roy. Astron. Soc.* **506**, 2871 (2021), arXiv:2010.03567 [astro-ph.IM].
- [45] J. Z. Chen, A. Upadhye, and Y. Y. Y. Wong, *JCAP* **04**, 078 (2021), code available at <https://github.com/joechenUNSW/gadget4-supereasy>, arXiv:2011.12504 [astro-ph.CO].
- [46] J. Riley *et al.* (COMPAS Team, Team COMPAS), *Astrophys. J. Supp.* **258**, 34 (2022), arXiv:2109.10352 [astro-ph.IM].
- [47] S. Stevenson, A. Vigna-Gómez, I. Mandel, J. W. Barrett, C. J. Neijssel, D. Perkins, and S. E. de Mink, *Nature Commun.* **8**, 14906 (2017), arXiv:1704.01352 [astro-ph.HE].
- [48] A. Vigna-Gómez *et al.*, *Mon. Not. Roy. Astron. Soc.* **481**, 4009 (2018), arXiv:1805.07974 [astro-ph.SR].
- [49] M. R. Mosbech, C. Boehm, and Y. Y. Y. Wong, (2022), arXiv:2207.03107 [astro-ph.CO].
- [50] E. D. Carlson, M. E. Machacek, and L. J. Hall, *Astrophys. J.* **398**, 43 (1992).
- [51] A. A. de Laix, R. J. Scherrer, and R. K. Schaefer, *Astrophys. J.* **452**, 495 (1995), arXiv:astro-ph/9502087 [astro-ph].
- [52] D. N. Spergel and P. J. Steinhardt, *Phys. Rev. Lett.* **84**, 3760 (2000), arXiv:astro-ph/9909386 [astro-ph].
- [53] R. Dave, D. N. Spergel, P. J. Steinhardt, and B. D. Wandelt, *Astrophys. J.* **547**, 574 (2001), arXiv:astro-ph/0006218 [astro-ph].
- [54] P. Creasey, O. Sameie, L. V. Sales, H.-B. Yu, M. Vogelsberger, and J. Zavala, *Mon. Not. Roy. Astron. Soc.* **468**, 2283 (2017), arXiv:1612.03903 [astro-ph.GA].
- [55] M. Rocha, A. H. G. Peter, J. S. Bullock, M. Kaplinghat, S. Garrison-Kimmel, J. Onorbe, and L. A. Moustakas, *Mon. Not. Roy. Astron. Soc.* **430**, 81 (2013), arXiv:1208.3025 [astro-ph.CO].
- [56] S. Y. Kim, A. H. G. Peter, and D. Wittman, *Mon. Not. Roy. Astron. Soc.* **469**, 1414 (2017), arXiv:1608.08630 [astro-ph.CO].
- [57] R. Huo, M. Kaplinghat, Z. Pan, and H.-B. Yu, *Phys. Lett. B* **783**, 76 (2018), arXiv:1709.09717 [hep-ph].
- [58] M. Markevitch, A. H. Gonzalez, D. Clowe, A. Vikhlinin, L. David, W. Forman, C. Jones, S. Murray, and W. Tucker, *Astrophys. J.* **606**, 819 (2004), arXiv:astro-ph/0309303 [astro-ph].
- [59] S. W. Randall, M. Markevitch, D. Clowe, A. H. Gonzalez, and M. Bradac, *Astrophys. J.* **679**, 1173 (2008), arXiv:0704.0261 [astro-ph].
- [60] K. Sigurdson, M. Doran, A. Kurylov, R. R. Caldwell, and M. Kamionkowski, *Phys. Rev. D* **70**, 083501 (2004), [Erratum: *Phys. Rev. D* **73**, 089903 (2006)], arXiv:astro-ph/0406355 [astro-ph].
- [61] R. J. Wilkinson, J. Lesgourgues, and C. Boehm, *JCAP* **1404**, 026 (2014), arXiv:1309.7588 [astro-ph.CO].
- [62] C. Boehm, J. A. Schewtschenko, R. J. Wilkinson, C. M. Baugh, and S. Pascoli, *Mon. Not. Roy. Astron. Soc.* **445**, L31 (2014), arXiv:1404.7012 [astro-ph.CO].
- [63] J. A. Schewtschenko, R. J. Wilkinson, C. M. Baugh, C. Boehm, and S. Pascoli, *Mon. Not. Roy. Astron. Soc.* **449**, 3587 (2015), arXiv:1412.4905 [astro-ph.CO].
- [64] J. A. Schewtschenko, C. M. Baugh, R. J. Wilkinson, C. Boehm, S. Pascoli, and T. Sawala, *Mon. Not. Roy. Astron. Soc.* **461**, 2282 (2016), arXiv:1512.06774 [astro-ph.CO].
- [65] M. Escudero, O. Mena, A. C. Vincent, R. J. Wilkinson, and C. Boehm, *JCAP* **1509**, 034 (2015), arXiv:1505.06735 [astro-ph.CO].
- [66] S. D. McDermott, H.-B. Yu, and K. M. Zurek, *Phys. Rev. D* **83**, 063509 (2011), arXiv:1011.2907 [hep-ph].
- [67] J. A. D. Diacoumis and Y. Y. Y. Wong, *JCAP* **1709**, 011 (2017), arXiv:1707.07050 [astro-ph.CO].
- [68] J. Stadler and C. Boehm, *JCAP* **1810**, 009 (2018), arXiv:1802.06589 [astro-ph.CO].
- [69] F.-Y. Cyr-Racine and K. Sigurdson, *Phys. Rev. D* **87**, 103515 (2013), arXiv:1209.5752 [astro-ph.CO].
- [70] A. D. Dolgov, S. L. Dubovsky, G. I. Rubtsov, and I. I. Tkachev, *Phys. Rev. D* **88**, 117701 (2013), arXiv:1310.2376 [hep-ph].
- [71] J. Stadler, C. Boehm, and O. Mena, *JCAP* **01**, 039 (2020), arXiv:1807.10034 [astro-ph.CO].
- [72] X.-l. Chen, S. Hannestad, and R. J. Scherrer, *Phys. Rev. D* **65**, 123515 (2002), arXiv:astro-ph/0202496 [astro-ph].
- [73] C. Dvorkin, K. Blum, and M. Kamionkowski, *Phys. Rev. D* **89**, 023519 (2014), arXiv:1311.2937 [astro-ph.CO].
- [74] A. A. Prinz *et al.*, *Phys. Rev. Lett.* **81**, 1175 (1998), arXiv:hep-ex/9804008 [hep-ex].
- [75] K. K. Boddy and V. Gluscevic, *Phys. Rev. D* **98**, 083510 (2018), arXiv:1801.08609 [astro-ph.CO].
- [76] T. R. Slatyer and C.-L. Wu, *Phys. Rev. D* **98**, 023013 (2018), arXiv:1803.09734 [astro-ph.CO].
- [77] W. L. Xu, C. Dvorkin, and A. Chael, *Phys. Rev. D* **97**, 103530 (2018), arXiv:1802.06788 [astro-ph.CO].
- [78] K. K. Boddy, V. Gluscevic, V. Poulin, E. D. Kovetz, M. Kamionkowski, and R. Barkana, *Phys. Rev. D* **98**, 123506 (2018), arXiv:1808.00001 [astro-ph.CO].
- [79] S. Das, R. Mondal, V. Rentala, and S. Suresh, *JCAP* **08**, 045 (2018), arXiv:1712.03976 [astro-ph.CO].
- [80] D. E. Kaplan, G. Z. Krnjaic, K. R. Rehermann, and C. M. Wells, *JCAP* **1005**, 021 (2010), arXiv:0909.0753 [hep-ph].

- [81] R. Diamanti, E. Giusarma, O. Mena, M. Archidiacono, and A. Melchiorri, *Phys. Rev. D* **87**, 063509 (2013), [arXiv:1212.6007 \[astro-ph.CO\]](#).
- [82] M. A. Buen-Abad, G. Marques-Tavares, and M. Schmaltz, *Phys. Rev. D* **92**, 023531 (2015), [arXiv:1505.03542 \[hep-ph\]](#).
- [83] J. Lesgourgues, G. Marques-Tavares, and M. Schmaltz, *JCAP* **1602**, 037 (2016), [arXiv:1507.04351 \[astro-ph.CO\]](#).
- [84] P. Ko, N. Nagata, and Y. Tang, *Phys. Lett. B* **773**, 513 (2017), [arXiv:1706.05605 \[hep-ph\]](#).
- [85] M. Escudero, L. Lopez-Honorez, O. Mena, S. Palomares-Ruiz, and P. Villanueva Domingo, *JCAP* **1806**, 007 (2018), [arXiv:1803.08427 \[astro-ph.CO\]](#).
- [86] S. Das and K. Sigurdson, *Phys. Rev. D* **85**, 063510 (2012), [arXiv:1012.4458 \[astro-ph.CO\]](#).
- [87] M. Archidiacono, D. C. Hooper, R. Murgia, S. Bohr, J. Lesgourgues, and M. Viel, *JCAP* **1910**, 055 (2019), [arXiv:1907.01496 \[astro-ph.CO\]](#).
- [88] M. Blennow, E. Fernandez-Martinez, O. Mena, J. Redondo, and P. Serra, *JCAP* **07**, 022 (2012), [arXiv:1203.5803 \[hep-ph\]](#).
- [89] F.-Y. Cyr-Racine, R. de Putter, A. Raccanelli, and K. Sigurdson, *Phys. Rev. D* **89**, 063517 (2014), [arXiv:1310.3278 \[astro-ph.CO\]](#).
- [90] S. Bose, M. Vogelsberger, J. Zavala, C. Pfrommer, F.-Y. Cyr-Racine, S. Bohr, and T. Bringmann, *Mon. Not. Roy. Astron. Soc.* **487**, 522 (2019), [arXiv:1811.10630 \[astro-ph.CO\]](#).
- [91] C. Boehm and P. Fayet, *Nucl. Phys. B* **683**, 219 (2004), [arXiv:hep-ph/0305261](#).
- [92] C. Boehm, Y. Farzan, T. Hambye, S. Palomares-Ruiz, and S. Pascoli, *Phys. Rev. D* **77**, 043516 (2008), [arXiv:hep-ph/0612228](#).
- [93] A. Olivares-Del Campo, C. Boehm, S. Palomares-Ruiz, and S. Pascoli, *Phys. Rev. D* **97**, 075039 (2018), [arXiv:1711.05283 \[hep-ph\]](#).
- [94] C. M. Baugh, C. G. Lacey, C. S. Frenk, G. L. Granato, L. Silva, A. Bressan, A. J. Benson, and S. Cole, *Mon. Not. Roy. Astron. Soc.* **356**, 1191 (2005), [astro-ph/0406069](#).
- [95] R. G. Bower, A. J. Benson, R. Malbon, J. C. Helly, C. S. Frenk, C. M. Baugh, S. Cole, and C. G. Lacey, *Mon. Not. Roy. Astron. Soc.* **370**, 645 (2006), [astro-ph/0511338](#).
- [96] H. Parkinson, S. Cole, and J. Helly, *Mon. Not. Roy. Astron. Soc.* **383**, 557 (2008), [arXiv:0708.1382](#).
- [97] C. D. P. Lagos, C. G. Lacey, C. M. Baugh, R. G. Bower, and A. J. Benson, *Mon. Not. Roy. Astron. Soc.* **416**, 1566 (2011), [arXiv:1011.5506](#).
- [98] A. J. Benson, A. Farahi, S. Cole, L. A. Moustakas, A. Jenkins, M. Lovell, R. Kennedy, J. Helly, and C. Frenk, *Mon. Not. Roy. Astron. Soc.* **428**, 1774 (2013), [arXiv:1209.3018](#).
- [99] J. Wang and S. D. M. White, *Mon. Not. Roy. Astron. Soc.* **380**, 93 (2007), [astro-ph/0702575](#).
- [100] M. R. Lovell, C. S. Frenk, V. R. Eke, A. Jenkins, L. Gao, and T. Theuns, *Mon. Not. Roy. Astron. Soc.* **439**, 300 (2014), [arXiv:1308.1399](#).
- [101] P. Norberg *et al.* (2dGRS), *Mon. Not. Roy. Astron. Soc.* **336**, 907 (2002), [arXiv:astro-ph/0111011](#).
- [102] S. P. Driver, A. S. G. Robotham, L. Kelvin, M. Alpaslan, I. K. Baldry, S. P. Bamford, S. Brough, M. Brown, A. M. Hopkins, J. Liske, J. Loveday, P. Norberg, J. A. Peacock, E. Andrae, J. Bland-Hawthorn, N. Bourne, E. Cameron, M. Colless, C. J. Conselice, S. M. Croom, L. Dunne, C. S. Frenk, A. W. Graham, M. Gunawardhana, D. T. Hill, D. H. Jones, K. Kuijken, B. Madore, R. C. Nichol, H. R. Parkinson, K. A. Pimbblet, S. Phillipps, C. C. Popescu, M. Prescott, M. Seibert, R. G. Sharp, W. J. Sutherland, E. N. Taylor, D. Thomas, R. J. Tuffs, E. van Kampen, D. Wijesinghe, and S. Wilkins, *Mon. Not. Roy. Astron. Soc.* **427**, 3244 (2012), [arXiv:1209.0259 \[astro-ph.CO\]](#).
- [103] I. Mandel and A. Farmer, *Phys. Rept.* **955**, 1 (2022), [arXiv:1806.05820 \[astro-ph.HE\]](#).
- [104] J. Riley, I. Mandel, P. Marchant, E. Butler, K. Nathaniel, C. Neijssel, S. Shortt, and A. Vigna-Gomez, *Mon. Not. Roy. Astron. Soc.* **505**, 663 (2021), [arXiv:2010.00002 \[astro-ph.SR\]](#).
- [105] J. Riley, I. Mandel, P. Marchant, E. Butler, K. Nathaniel, C. Neijssel, S. Shortt, and A. Vigna-Gomez, “Chemically Homogeneous Evolution: A rapid population synthesis approach,” <https://doi.org/10.5281/zenodo.5595426> (2021).
- [106] C. J. Neijssel, A. Vigna-Gómez, S. Stevenson, J. W. Barrett, S. M. Gaebel, F. Broekgaarden, S. E. de Mink, D. Szécsi, S. Vinciguerra, and I. Mandel, *Mon. Not. Roy. Astron. Soc.* **490**, 3740 (2019), [arXiv:1906.08136 \[astro-ph.SR\]](#).
- [107] J. Abadie *et al.* (LIGO, Virgo), *Class. Quant. Grav.* **27**, 173001 (2010), [arXiv:1003.2480 \[astro-ph.HE\]](#).
- [108] R. O’Leary, R. W. O’Shaughnessy, and F. Rasio, *Phys. Rev. D* **76**, 061504 (2007), [arXiv:astro-ph/0701887](#).
- [109] M. C. Miller and V. M. Lauburg, *Astrophys. J.* **692**, 917 (2009), [arXiv:0804.2783 \[astro-ph\]](#).
- [110] B. McKernan *et al.*, *Astrophys. J.* **866**, 66 (2018), [arXiv:1702.07818 \[astro-ph.HE\]](#).
- [111] S. Bird, I. Cholis, J. B. Muñoz, Y. Ali-Haïmoud, M. Kamionkowski, E. D. Kovetz, A. Raccanelli, and A. G. Riess, *Phys. Rev. Lett.* **116**, 201301 (2016), [arXiv:1603.00464 \[astro-ph.CO\]](#).
- [112] R. Abbott *et al.* (LIGO, Virgo, KAGRA), (2021), [arXiv:2111.03634 \[astro-ph.HE\]](#).
- [113] M. Martinelli, F. Scardella, N. B. Hogg, B. J. Kavanagh, D. Gaggero, and P. Fleury, (2022), [arXiv:2205.02639 \[astro-ph.CO\]](#).
- [114] M. Maggiore *et al.*, *JCAP* **03**, 050 (2020), [arXiv:1912.02622 \[astro-ph.CO\]](#).
- [115] M. Evans *et al.*, (2021), [arXiv:2109.09882 \[astro-ph.IM\]](#).
- [116] J. W. Barrett, S. M. Gaebel, C. J. Neijssel, A. Vigna-Gómez, S. Stevenson, C. P. L. Berry, W. M. Farr, and I. Mandel, *Mon. Not. Roy. Astron. Soc.* **477**, 4685 (2018), [arXiv:1711.06287 \[astro-ph.HE\]](#).
- [117] F. S. Broekgaarden *et al.*, *Mon. Not. Roy. Astron. Soc.* (2022), [10.1093/mnras/stac1677](#), [arXiv:2112.05763 \[astro-ph.HE\]](#).
- [118] J. P. Gardner *et al.*, *Space Sci. Rev.* **123**, 485 (2006), [arXiv:astro-ph/0606175](#).
- [119] R. E. Angulo, O. Hahn, and T. Abel, *Mon. Not. Roy. Astron. Soc.* **434**, 3337 (2013), [arXiv:1304.2406 \[astro-ph.CO\]](#).
- [120] O. Hahn and R. E. Angulo, *Mon. Not. Roy. Astron. Soc.* **455**, 1115 (2016), [arXiv:1501.01959 \[astro-ph.CO\]](#).
- [121] J. Stücker, R. E. Angulo, O. Hahn, and S. D. M. White, *Mon. Not. Roy. Astron. Soc.* **509**, 1703 (2021), [arXiv:2109.09760 \[astro-ph.CO\]](#).

- [122] M. R. Lovell, C. S. Frenk, V. R. Eke, A. Jenkins, L. Gao, and T. Theuns, *Mon. Not. Roy. Astron. Soc.* **439**, 300 (2014), [arXiv:1308.1399 \[astro-ph.CO\]](#).
- [123] M. R. Lovell, *Astrophys. J.* **897**, 147 (2020), [arXiv:2003.01125 \[astro-ph.CO\]](#).
- [124] P. Ajith *et al.*, *Phys. Rev. D* **77**, 104017 (2008), [Erratum: *Phys.Rev.D* 79, 129901 (2009)], [arXiv:0710.2335 \[gr-qc\]](#).
- [125] R. Abbott *et al.* (LIGO, Virgo), *Astrophys. J. Lett.* **913**, L7 (2021), [arXiv:2010.14533 \[astro-ph.HE\]](#).

Appendix A: SUPPLEMENTAL MATERIAL

N-body simulations and the halo mass function

Our simulations are performed using a modified version of GADGET-4 [44], which includes massive neutrinos via the SUPEREASY linear response method of [45]. GADGET-4 is a massively parallel N-body code supporting both collisionless (gravity-only) simulations and hydrodynamical simulations for baryonic matter and star formation. We restrict ourselves to collisionless simulations, which suffice for the purpose of cross-checking the GALFORM halo mass function output. Initial conditions are generated at $z = 49$ using the built-in NGENIC implementation, with linear matter power spectra from our modified version of CLASS as input. For interaction strengths allowed by current cosmological data, dark matter-neutrino decoupling happens at redshifts $z \gg 1000$, well before the simulation initialisation time. Thus, the interaction affects non-linear structure formation only through initial conditions, and there is no need to modify the main body of GADGET-4 itself.

To probe the effects of our IDM scenario at a range of scales, we run our simulations using $N = 512^3$ particles in several different box sizes, $(50\text{Mpc})^3$, $(100\text{Mpc})^3$, $(500\text{Mpc})^3$, and $(1\text{Gpc})^3$, for different values of the interaction strength $u_{\nu\chi}$, including a non-interacting ($u_{\nu\chi} = 0$) set. All other cosmological parameters are kept fixed to the CMB+BAO best-fit values found in [38]. We also perform a set of simulations using the best-fit parameters found in [39], which is phenomenologically similar to our $u_{\nu\chi} = 3.4 \times 10^{-6}$ scenario.

We use the friends-of-friends algorithm to identify halos in our simulations. For halo masses we use the convention M_{200c} , i.e., the mass contained within a sphere with mean density 200 times the critical density of the universe. The halos from each simulation are sorted into 30 evenly-spaced logarithmic mass bins to obtain the halo number density per mass bin, i.e., the halo mass function. As is well described in the literature (see, e.g., [99, 100, 119–121]), the halo mass function of cosmologies with a small-scale cut-off exhibits unphysical discreteness effects on small scales (relative to the box size). We therefore conservatively choose to disregard the low-mass end of each halo mass function thus constructed, cutting it off just above the scale at which discreteness effects become evident. Then, to produce a halo mass function that spans a range of mass scales, we simply stitch together the pieces obtained from our different box-size runs.

We have attempted to describe the IDM halo mass functions semi-analytically using the Sheth-Tormen mass function, with the IDM linear matter power spectra as input and a real-space spherical tophat filter for smoothing. However, as is evident in Fig. 6, the Sheth-Tormen mass function thus constructed fails to capture the low-mass

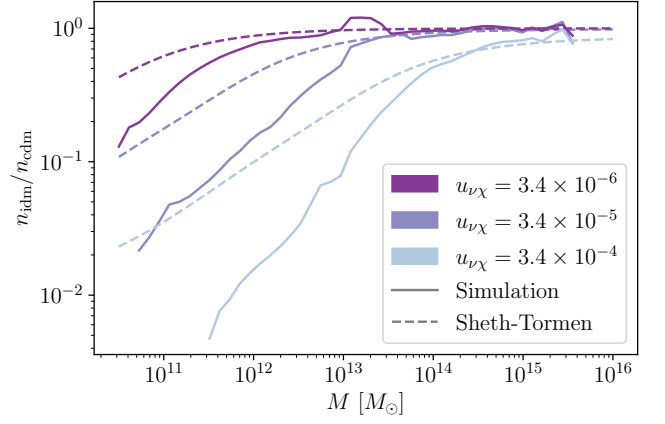


Figure 6. IDM halo mass function n_{idm} normalised to a reference CDM mass function n_{cdm} for various interacting strengths $u_{\nu\chi}$, computed from N-body simulations (solid lines) and the Sheth-Tormen formalism (dashed lines). The choice of $u_{\nu\chi} = 3.4 \times 10^{-4}$ has been motivated by the CMB+BAO constraint found in Ref. [38]. It is evident that the standard Sheth-Tormen halo mass function does not provide a good description of our simulation results.

suppression relative to the CDM case seen in our N-body simulation results. We therefore forego the Sheth-Tormen approach completely, opting instead to use a fitting function to describe the suppression relative to the CDM case.

We find the following fitting function to serve the purpose well:

$$\frac{n_{\text{idm}}}{n_{\text{cdm}}} = \frac{1}{1 + \left(\frac{M_\beta}{M}\right)^\alpha}, \quad (\text{A1})$$

where $M_\beta \equiv (4\pi)\bar{\rho}_m/3k_\beta^{-3}$ is the mass corresponding to the wave number k_β at which the linear matter power spectrum of an IDM scenario is suppressed by $\beta\%$ relative to the CDM case, $\bar{\rho}_m$ is the comoving mean matter density, and the parameters α and β are to be determined by fitting Eq. (A1) to our N-body results. The fit is achieved by forming and then minimising a figure-of-merit (FoM) of the form

$$\text{FoM} = \sum_M \left(\log_{10} \left(\frac{n_{\text{idm}}}{n_{\text{cdm}}} \right)_{\text{fit}} - \log_{10} \left(\frac{n_{\text{idm}}}{n_{\text{cdm}}} \right)_{\text{N-body}} \right)^2, \quad (\text{A2})$$

and fitting Eq. (A1) to our $u_{\nu\chi} = 3.4 \times 10^{-4}$, 3.4×10^{-5} , and 3.4×10^{-6} simulation results simultaneously.

We find the best-fit values to be $\alpha = 0.9$ and $\beta = 10$. The fit is displayed against simulation results in Fig. 7. We also give in Table I the M_{10} values corresponding to several interacting strengths $u_{\nu\chi}$. To confirm the robustness of the fit, we test the fitting function (A1) against simulations at several low $u_{\nu\chi}$ values outside of the calibration range, and find the fit to be accurate to better than $\sim 10\%$.

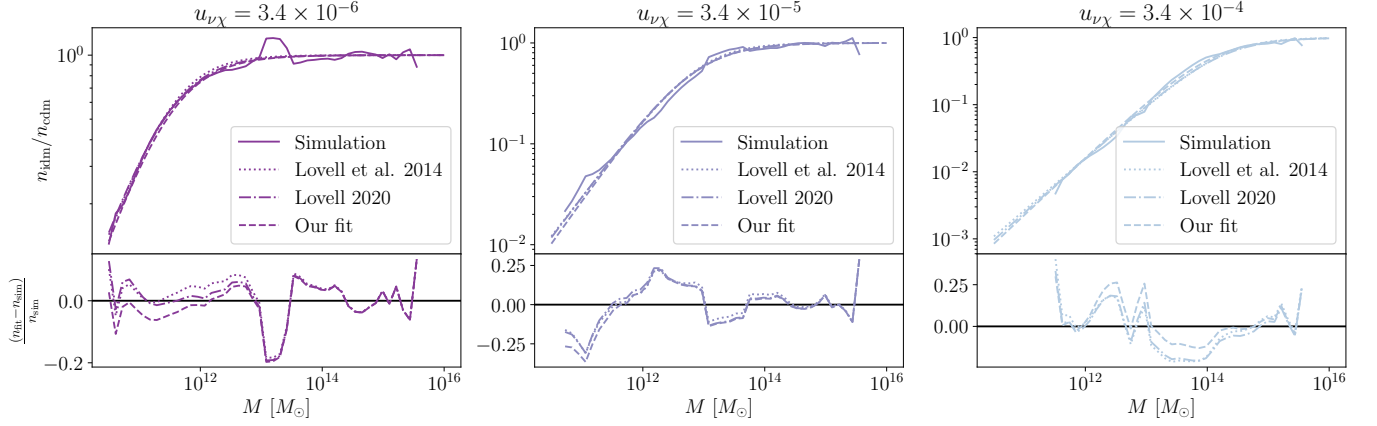


Figure 7. IDM halo mass function n_{idm} normalised to a reference CDM mass function n_{cdm} for three interacting strengths $u_{\nu\chi}$. Solid lines denote results from N-body simulations; dashed lines represent our fitting function (A1); dotted and dot-dash lines are two fitting functions from Refs. [122, 123]. The bottom panel of each plot shows the fractional residuals of the three fitting functions.

$u_{\nu\chi}$	M_{10}/M_{\odot}
3.4×10^{-4}	1.0×10^{14}
3.4×10^{-5}	5.3×10^{12}
3.4×10^{-6}	2.3×10^{11}
3.4×10^{-7}	8.3×10^9
3.4×10^{-8}	2.9×10^8
3.4×10^{-9}	9.6×10^6

Table I. IDM interacting strengths and the corresponding suppression mass scale M_{β} that appears in the fitting function (A1) for the halo mass function. We find $\beta = 10$ to be the best-fit value against simulation results.

Finally, we remark that extended Press-Schechter formalism used in `GALFORM` does not exactly use our fitting function, but produces a halo mass function that matches it to the same or better precision, as the fitting function matches the simulations.

Gravitational-wave detection forecasts

We choose some redshift threshold z_* , and define $N_{>}(z_*)$ as the number of detected BBHs whose best-fit inferred redshift falls above this threshold, $\hat{z} > z_*$. Based on our work, different dark matter scenarios will predict different values of $N_{>}$. We can predict whether these models are distinguishable in a given observational scenario by forecasting the corresponding uncertainty on $N_{>}$.

It is straightforward to write down the mean value of

this quantity,

$$\begin{aligned} \bar{N}_{>}(z_*) &= T_{\text{obs}} \int_0^\infty dz \frac{dV}{dz} \frac{\bar{\mathcal{R}}(z)}{1+z} \\ &\times \int d\theta p_{\text{pop}}(\theta|z) p_{\text{det}}(z, \theta) p_{>}(z, \theta|z_*). \end{aligned} \quad (\text{A3})$$

Here, T_{obs} is the total observing time, V is the comoving volume as a function of redshift, $\bar{\mathcal{R}}$ is the mean BBH merger rate density as a function of redshift, θ is a vector of BBH parameters (masses, spins, etc.) with population distribution $p_{\text{pop}}(\theta|z)$ (which we allow to evolve over redshift), $p_{\text{det}}(z, \theta)$ is the probability of detecting a BBH with parameters θ at redshift z , and $p_{>}(z, \theta|z_*)$ is the probability of inferring a best-fit redshift greater than z_* for the same BBH. We will revisit how to calculate these probabilities below.

In order to calculate the variance of $N_{>}$, we assume that the number, n , of BBH signals emitted from a comoving volume V in a source-frame time $T = T_{\text{obs}}/(1+z)$ is a Poisson random variable with mean $\bar{n} = VT\bar{\mathcal{R}}$. We further assume that Poissonian fluctuations in the BBH rate at different redshifts are uncorrelated with each other. This allows us to write the covariance matrix between these BBH number counts as

$$\text{Cov}[n(z), n(z')] = \delta(z - z') \text{Var}[n(z)] = \delta(z - z') \bar{n}(z). \quad (\text{A4})$$

We thus find that

$$\begin{aligned} \text{Var}[N_{>}(z_*)] &= T_{\text{obs}} \int_0^\infty dz \frac{dV}{dz} \frac{\bar{\mathcal{R}}(z)}{1+z} \\ &\times \left[\int d\theta p_{\text{pop}}(\theta|z) p_{\text{det}}(z, \theta) p_{>}(z, \theta|z_*) \right]^2, \end{aligned} \quad (\text{A5})$$

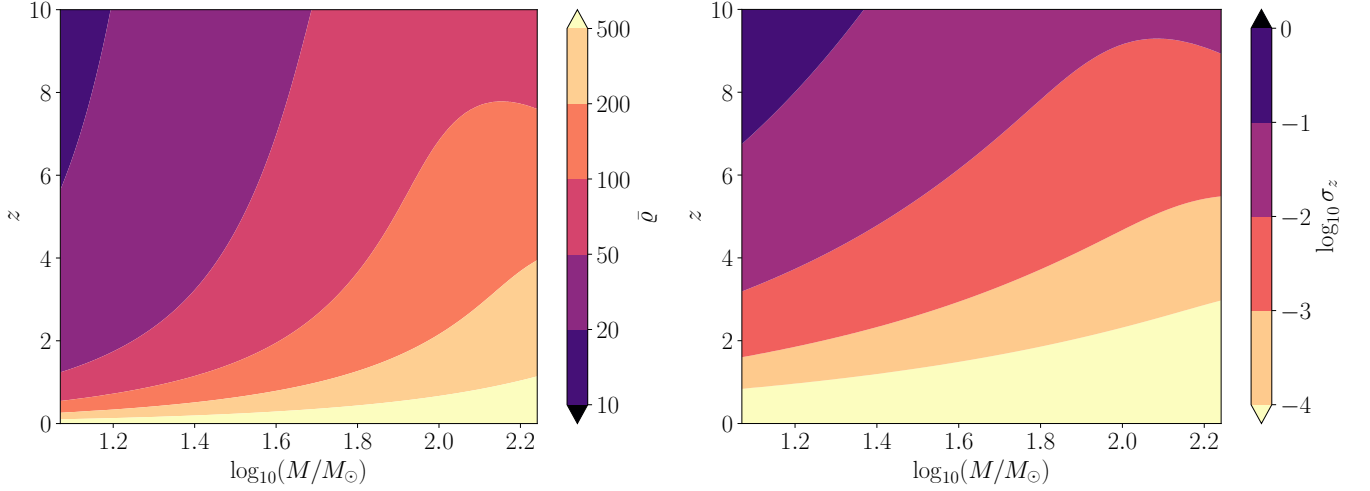


Figure 8. Left panel: mean signal-to-noise ratio $\bar{\rho} = \sqrt{\langle h|h \rangle}$ of equal-mass non-spinning BBHs detected with our third-generation interferometer network, as a function of redshift z and total source-frame mass M . Right panel: forecast redshift uncertainty $\sigma_z = \sqrt{(F^{-1})_{zz}}$ for the same parameter space. The mass range in both panels is truncated at the boundaries of our broken-power-law mass distribution ($12 M_{\odot} < M < 174 M_{\odot}$).

which shows that $N_{>}$ is *not* itself Poissonian, since its mean and variance are unequal so long as the θ integral is less than unity.

We assume the BBH signals are detected using a matched-filter search, in which the detection statistic is a noise-weighted inner product of the data d with the signal template h ,

$$(d, h) \equiv 4 \operatorname{Re} \int_0^{\infty} df \frac{\tilde{d}(f) \tilde{h}^*(f)}{S(f)}, \quad (\text{A6})$$

with $S(f)$ the noise power spectral density of the detector. In Gaussian noise, the signal-to-noise ratio (SNR) ρ of the search is then approximately a Gaussian random variable with unit variance and mean $\bar{\rho} = \sqrt{\langle h, h \rangle}$; so for example, having $\bar{\rho} = 5$ would constitute a 5σ detection in this idealised scenario. In reality, the noise is not Gaussian, and we require a larger SNR in order to confidently discriminate a BBH from various non-Gaussian noise transients. A commonly-adopted detection threshold is $\bar{\rho} \geq 8$. We can therefore write the detection probability as

$$\begin{aligned} p_{\text{det}}(z, \theta) &= \int_8^{\infty} \frac{d\rho}{\sqrt{2\pi}} \exp\left[-\frac{1}{2}(\rho - \bar{\rho}(z, \theta))^2\right] \\ &= \frac{1}{2} \left[1 + \operatorname{erf}\left(\frac{\bar{\rho}(z, \theta) - 8}{\sqrt{2}}\right) \right], \end{aligned} \quad (\text{A7})$$

which interpolates between (almost) zero for faint signals and (almost) one for strong signals, with a characteristic width set by the randomness of the observed SNR.

We approximate the redshift inference using a Fisher forecast. The Fisher matrix for parameters θ_i (including z) of the signal model $h(\theta_i)$ is given by

$$F_{ij} \equiv \left(\frac{\partial h}{\partial \theta_i}, \frac{\partial h}{\partial \theta_j} \right). \quad (\text{A8})$$

In the strong-signal limit, the inferred redshift \hat{z} is a Gaussian random variable with mean equal to the true redshift z , and standard deviation given by the inverse Fisher matrix,

$$\sigma_z(z, \theta) = \sqrt{(F^{-1})_{zz}}. \quad (\text{A9})$$

We therefore have

$$p_{>}(z, \theta|z_*) = \frac{1}{2} \left[1 + \operatorname{erf}\left(\frac{z - z_*}{\sqrt{2}\sigma_z}\right) \right], \quad (\text{A10})$$

which interpolates between (almost) zero for nearby BBHs and (almost) one for distant BBHs, with a width set by σ_z .

In order to evaluate the expected SNR $\bar{\rho}$ and the redshift uncertainty σ_z , we need a signal model $h(\theta, z)$. For this, we use the phenomenological hybrid waveform model of [124]. For simplicity, we assume that the BBHs are all equal-mass and non-spinning (as is approximately true for most of the BBHs detected by LIGO/Virgo thus far [112]), and we average out all of the extrinsic parameters (sky location, polarisation angle, inclination, etc.). This reduces the number of relevant parameters to just two: the redshift z and the total mass M . In terms of these parameters, the frequency-domain waveform model can be

written as

$$\begin{aligned}
\tilde{h}(f) &= e^{i\Psi(f)} \left(\frac{\pi}{30} \right)^{1/2} \frac{(GM)^2}{2r} (\pi GM f_{\text{merg}})^{-7/6} \\
&\times \begin{cases} (f/f_{\text{merg}})^{-7/6} & f < f_{\text{merg}} \\ (f/f_{\text{merg}})^{-2/3} & f_{\text{merg}} \leq f < f_{\text{ring}} , \\ \frac{(f_{\text{ring}}/f_{\text{merg}})^{-2/3} f_{\text{width}}^2}{(f-f_{\text{ring}})^2 + f_{\text{width}}^2} & f_{\text{ring}} \leq f < f_{\text{cut}} \end{cases} \\
\Psi(f) &= \varphi_0 + \sum_{k=0}^7 \psi_k (\pi GM f)^{(k-5)/3},
\end{aligned} \tag{A11}$$

where f_{merg} , f_{ring} , f_{cut} , f_{width} , φ_0 , and $\{\psi_k\}$ are all constants given in [124]. This expression is appropriate for $z \rightarrow 0$; in order to generalise to arbitrary red-

shift we simply replace $r \rightarrow d_L(z)$, $M \rightarrow (1+z)M$, and $f \rightarrow f/(1+z)$ for all of the frequencies.

We can now use this waveform to compute the expected SNR $\bar{\rho}$ and the redshift uncertainty σ_z (the latter of which involves computing and inverting the 2×2 Fisher matrix for the mass and redshift), as shown in Fig 8. The final missing ingredient to calculate $N_{>}$ and its variance is the population distribution of the BBH masses, for which we use the best-fit broken-power-law model from [125], which transitions from a shallow $m^{-1.58}$ power law at low masses ($5.9 M_{\odot} < m < 41 M_{\odot}$) to a steeper one, $m^{-5.59}$, at large masses ($41 M_{\odot} < m < 87 M_{\odot}$). Here m is the source-frame mass of each individual black hole, so $M = 2(1+z)m$.